IEEE Access
Multidisciplinary ⋮ Rapid Review ⋮ Open Access Journal

Received 21 October 2023, accepted 3 November 2023, date of publication 8 November 2023, date of current version 13 November 2023.

Digital Object Identifier 10.1109/ACCESS.2023.3331500

RESEARCH ARTICLE

Development of a Smart Spinal Epidural Needle Based on Load Cell Sensors

MURAD ALTHOBAITI[1], YARA ALAGLI[1], NAJWA ALZAHRANI[1], SARA ALZAHRANI[1], SAJID ALI[2], NASIR G. HARIRI[2], KAMRAN HAMEED[1], AND IBRAHEEM AL-NAIB[3,4], (Senior Member, IEEE)

[1]Biomedical Engineering Department, College of Engineering, Imam Abdulrahman Bin Faisal University, Dammam 34212, Saudi Arabia
[2]Department of Mechanical and Energy Engineering, College of Engineering, Imam Abdulrahman Bin Faisal University, Dammam 34212, Saudi Arabia
[3]Bioengineering Department, King Fahd University of Petroleum & Minerals, Dhahran 31261, Saudi Arabia
[4]Interdisciplinary Research Center of Communication Systems and Sensing, King Fahd University of Petroleum & Minerals, Dhahran 31261, Saudi Arabia

Corresponding author: Murad Althobaiti (mmalthobaiti@iau.edu.sa)

This work was supported by the Deputyship for Research and Innovation, Ministry of Education of Saudi Arabia, through Imam Abdulrahman Bin Faisal University/College of Engineering, under Project IF-2022-046-Eng.

ABSTRACT In this article, we have developed a high-accuracy and low-cost smart epidural needle system. It is based on force puncture sensing and guidance mechanism that enhances success rate and reduces the risks of accidental punctures. The design incorporates a subminiature load cell embedded in the spinal needle which measures the force exerted by each tissue layer on the needle tip. By identifying the force range for each layer, the needle can be safely inserted and accurately reach the targeted area. Accordingly, a classifier model for this identification process was developed and tested. More than a hundred experimental readings were collected and used for training the developed classifier model of the system. Furthermore, a phantom with six spinal cord layers, that mimics the properties of different spinal tissue layers, was built and utilized for testing purposes. The experimental results of the developed smart spinal epidural needle system highlight the ability of the system to identify the needle location with an accuracy of about 86.7%. Hence, it provides promising outcomes and a feasible solution for the future development of spinal epidural needle systems.

INDEX TERMS Epidural space, spinal needle, load sensor, epidural anesthesia, force measurements.

I. INTRODUCTION

Spinal epidural needles are commonly used to provide pain relief for labor and certain surgeries. For this purpose, they are injected into the epidural space (ES). Given the delicate nature of the spinal cord, the identification of the ES is required to ensure patient safety. This procedure is dependent on the skills of the physicians to detect changes in the force exerted on the needle as they push it through different layers of tissues. Hence, there is a good chance for mistakes that could cause lumbar trauma [1], [2]. Therefore, various technologies utilizing highly sensitive electrical and optical components to detect the targeted spinal layer have been developed. Force-detection technique was introduced by Dogliotti [3] in 1933, which is known as the Loss of Resistance (LOR) technique. This technique uses a bevel-tip needle that is connected to a syringe filled with physiological solution inserted with constant pressure on the piston as it penetrates the ligamentum flavum (LF). As soon as the needle passes the subcutaneous tissue, it encounters resistance in the supraspinous ligaments due to the density of this area and the needle's bevel tip. Then, the needle is advanced through the LF, where a strong resistance to the injected needle occurs. However, the resistance is diminished as the needle arrives at the ES. The reason behind this rapid decrease in resistance is due to the abundance of loose adipose connective tissue that is filled with blood vessels [3]. Another idea was proposed using the Fiber Bragg Grating Force Device (FBGFD) to monitor the exerted force by the spinal needle during Lumbar Puncture (LP) [4]. In general, FBG sensors are widely used in biomedical applications since they are small in size, inert, provide high sensitivity, insensitive to radio frequency, and have immunity to electromagnetic interference [5]. FBG sensor is deployed along the length

The associate editor coordinating the review of this manuscript and approving it for publication was Santosh Kumar.

of an optical fiber and fabricated by inscribing a periodic refractive index change in the core of the optical fiber. The FBG is affected if an axial strain is induced, which causes a proportional shift in the Bragg wavelength. The strain values can be easily obtained by calibrating the instrument. Furthermore, certain imaging techniques were proposed such as optical coherence tomography, ultrasound, and fluoroscopy [6], [7], [8], [9]. Nevertheless, various techniques suffer from different limitations. For instance, in the fluoroscopy technique, the differentiation of soft tissues such as blood vessels and nerves was not applicable which decreased the effectiveness of the results. More recently, convolutional neural networks (CNN) were used as a classification tool to improve tissue recognition and enhance the differentiation of different layers [5]. The thickness of the soft tissues affects the viscoelastic measures of the soft tissues over the bones, as has been demonstrated [10]. This requires delivering a mechanical stimulation to the tissue in question and examining the ensuing force and motion responses, which vary greatly between diverse biological materials. Simpson et al. [11] described a method for anticipating an impending bone hit as an implementation of this concept. By assessing the mechanical characteristics of the tissue before inserting the epidural needle, this technique enables the needle to be anticipatorily guided and the strike to be avoided.

Using ultrasound imaging of anatomical markers, the process may be guided in real time. Ultrasound can be used to measure the depth of the ES and the angle at which the needle is inserted [12], [13]. In contrast to preprocedural scanning, real-time ultrasonography may be more precise since it is not affected by changes in the patient's posture [1]. Only at a distance of around 2 mm may fiber optic methods be employed, which is too near for them to be useful in avoiding bone hits [14], [15]. In recent years, the use of haptic devices in medical simulations has increased, offering an accurate means of simulating the sensation of operation [16], [17]. Simple epidural simulators have evolved and improved since their original publication in 1980. Mediseus [18] presents a computer-based simulator, which connects to computers with visual screens and uses haptic feedback devices housed in portable enclosures. Mediseus and other devices have been criticized for lacking measurable data for force feedback [19].

In this paper, a new spinal needle that utilizes different tissue forces to guide the physician during needle insertion has been designed. It employs a very compact load cell embedded in the spinal needle to measure the force of each layer based on the change of the strain gauge. The range of the force for each layer helps the spinal needle insertion into ES. A spinal phantom was prepared to test the force caused by each layer. Moreover, the variation of the force value was studied, where it was found that the force of the LF, interspinous ligament (IL), muscle, fat, skin, and ES from high to low, respectively. This design showed a high accuracy in identifying different layers.

II. DESIGN AND METHODOLOGY

A. CONCEPTUAL DESIGN OF THE NEEDLE

The basic conceptual design of the needle is illustrated in Fig. 1(a), where the 3D views of the proposed design are shown. The presented novel design utilizes outer and inner needles, a spring that is placed between the two needles, and a force-measuring sensor.

The assembled and exploded views of the epidural needle design are demonstrated in Fig. 1(b). The designed epidural needle functions as a spring-pushed-based device, where the spring is in between the outer needle and the inner needle. The casing in which the outer needle is placed is attached to a force-measuring sensor from the rare end. The outer needle, when inserted into the membrane surrounding the cerebral spinal fluid (CSF), will be pushed back due to the resistance it encounters from the different tissues before it reaches the CSF. This pressure experienced by the needle will be transmitted to the force-measuring sensor via the spring and the inner needle attachment. Once the outer needle enters the CSF, the force sensor will feature a significant pressure drop. This pressure drop will be used as an indication that the needle has reached the ES. At this point, the inner needle along with its attachment will be removed, and the sample will be collected accordingly.

B. LOAD CELL SELECTION

The proposed needle is built based on force detection of different tissue resistances on the spinal needle. The selected load cell was a subminiature button load cell, manufactured by ATO [20]. This load cell is distinguished by its compact size and low price. The subminiature load cell displays a high sensitivity, and smaller size, at a lower price. In terms of the operating temperature, the button load cell does in fact operate in a smaller range. However, the environment in which the device is meant to be used (hospitals) is generally temperature controlled. Therefore, the temperature advantage of the other high precision load cells (such as MDB-5 Ultra Precision, manufactured by Transducer Techniques) is not of great significance. Since the main goal is to design an efficient force-identification spinal needle that is efficiently designed, light weight, and low cost, the button load cell was selected. Although the MDB-5 has better features than the subminiature load cell, the latter displays satisfactory characteristics for our given application and was selected due to its advantage of being smaller in size and lighter in weight than the former, allowing the device to be more ergonomic [21].

C. PHANTOM DESIGN

To test and train the classification system, a phantom was created. The phantom was made up of six layers: skin, muscle, subcutaneous fat, IL, LF, and ES, each of which has distinct properties. Based on the idea in [22], the layers were created using various meat cuts and gelatin, with the powder-to-water

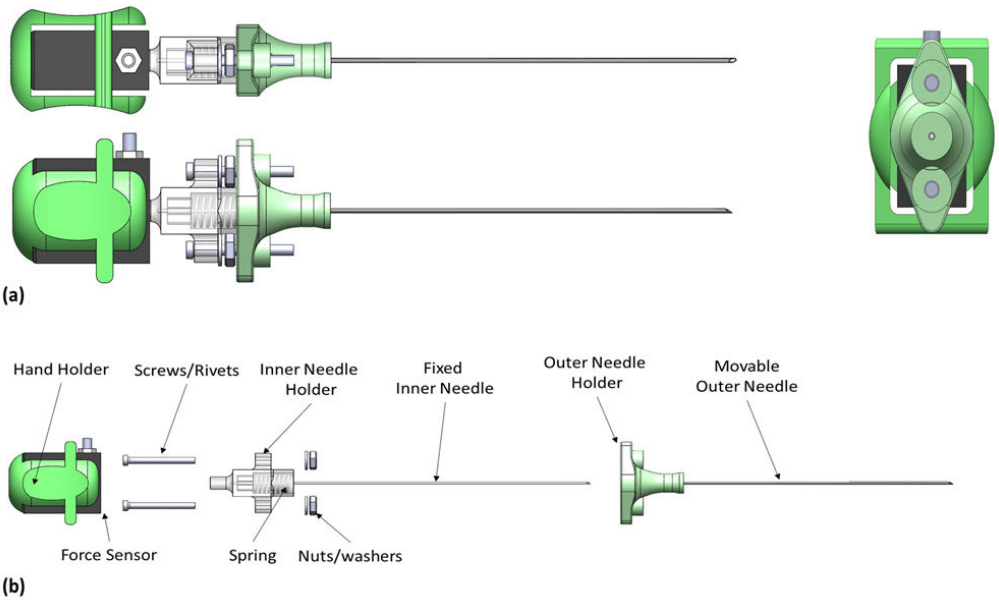

FIGURE 1. (a) 3D-views of the proposed design, (b) detailed 2-D drawing of the spinal epidural needle.

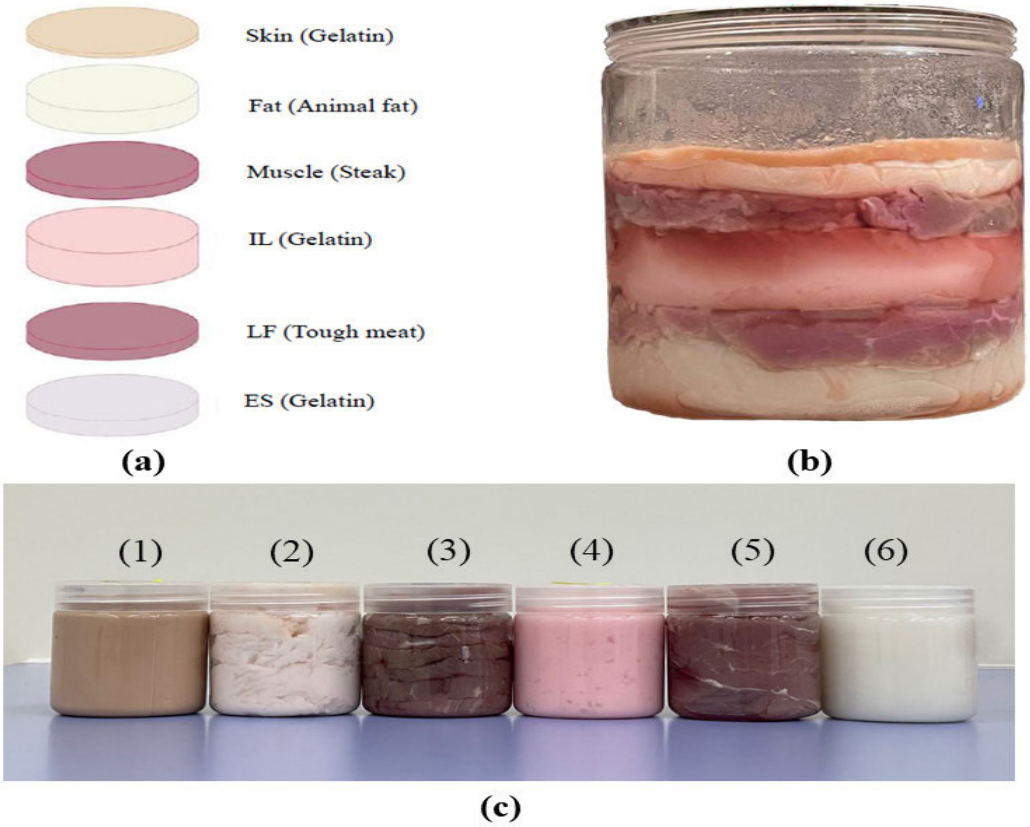

FIGURE 2. (a) Proposed phantom design, (b) Complete designed phantom and (c) Individual Phantom Layers: (1) Skin, (2) Fat, (3) Muscle, (4) IL, (5) LF and (6) ES.

ratio changing for each layer in order to alter the gelatin layers' consistencies. The tissues were further colored to reflect a hue resembling that of genuine tissues. The ES had the most water since it had the least resistance of the six layers, whereas the skin layer had the highest gelatin-to-water ratio to mimic the flexibility of real skin. Regarding the IL,

TABLE 1. Calibration results of the load cell.

Load [g]	Voltage [V]
0	0.4312
100	0.5074
200	0.5684
300	0.6370
400	0.7007
500	0.7939
600	0.8330
700	0.9016
800	0.9702
900	1.0388
1000	1.1123

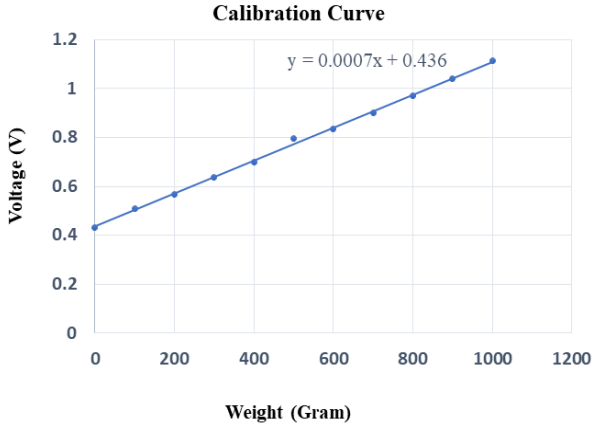

FIGURE 3. Calibration curve of the load cell.

the skin and ES were separated by the same amount of gelatin in water. The muscle was modeled using beef steak, while the LF was modeled using beef striploin, which is harder and has higher resistance. Fig. 2(a) depicts the intended phantom design, while Fig. 2(b) depicts the implemented phantom. Experimentation and data gathering were carried out on each layer individually, as shown in Fig. 2(c) below.

D. CALIBRATION OF THE LOAD CELL

Before collecting data from the load cell, it should be calibrated. The calibration equation was derived by relating the weight in grams, that was mounted up the load cell, to the output voltage, as seen in Table 1. The calibration was carried out in LabVIEW, where the output voltage was collected from the analog pin of the Arduino, which was used to monitor the output voltage when the weight was changed. The following calibration equation was obtained from the linear calibration curve in Fig. 3:

$$\begin{aligned}\text{Weight (Newton)} &= \text{Weight (Gram)} \times 9.81 \times 10^{-3} \\ &= \left(\frac{\text{Voltage} - 0.436}{0.0007}\right) \times 9.81 \times 10^{-3}\end{aligned}$$

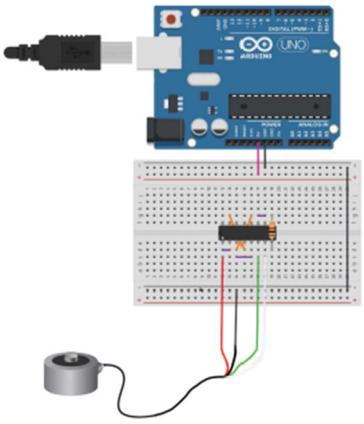

FIGURE 4. Data collection circuit.

The full method, however, was completed in MATLAB for additional processing.

E. DETAILED DESCRIPTION OF THE FINAL DESIGN

The proposed prototype is made up of three primary controlling hardware components. The data collection circuit, shown in Fig. 4, is built using an instrumentation amplifier (INA125P), a resistor (6.8 Ω), and an Arduino Uno board, which is utilized to gather input and power the other components as shown in Fig. 5. The instrumentation amplifier is also linked to the load cell, which is located inside the needle housing. The system software is the second component, which was created with MATLAB and the Arduino IDE. To compile and upload the code needed to acquire data, program the LCD display, and program the push buttons used to turn on and off the screen, the Arduino IDE was utilized. MATLAB was used in the meantime to gather data, filter readings, extract features, train classifiers, display graphs, and classify fresh signals into one of six spinal layers. The detailed code for the data acquisition, module training, and software classification can be found in appendices A, B, & C; respectively.

The final component required to build the system is the display and pushbutton circuit. Fig. 6 depicts this circuit, that is built using an Arduino Due board, two pushbuttons, an ILI9488 TFT display, and some resistors. The Arduino features an ILI9488 TFT display, its board is connected to the ILI9488 TFT display, and the pushbuttons are hooked to the digital inputs. The first push-button turns on/off the screen, while the second starts and stops the MATLAB system.

F. CHARACTERIZATION OF DIFFERENT FEATURES OF SPINAL LAYERS

The experimental setup used to acquire readings and test the classification is viewed in Fig. 7. The setup included the components mentioned in Section II-D. The data acquisition board was connected to the computer in order to interface the software and the hardware in order to classify the readings. Initially, during experimentation, the results were displayed on the computer screen for ease of access. However, in the

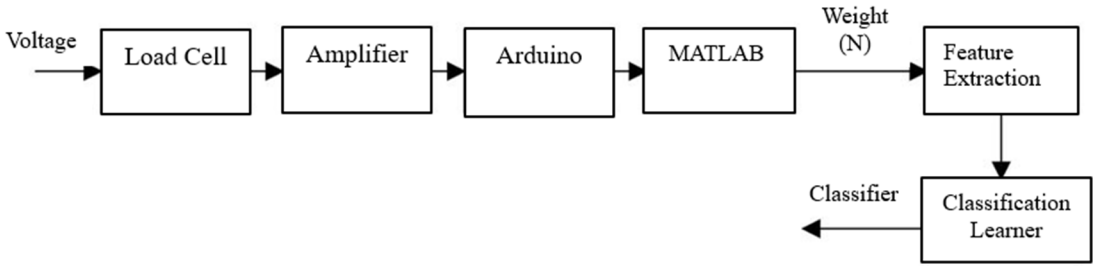

FIGURE 5. Block diagram for data acquisition system.

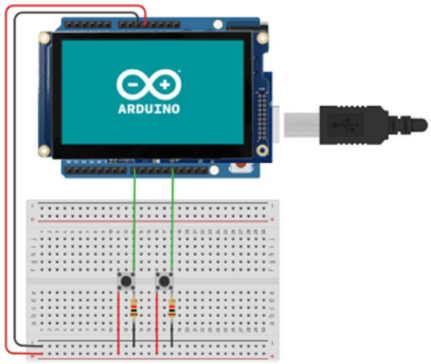

FIGURE 6. Display circuit.

final prototype, the results are displayed on a separate, standalone display screen. To begin with, the calibration equation obtained from the initial testing was written in MATLAB so that each reading is automatically converted to Newtons to evaluate it. Then, as seen in Fig. 7, the needle with the force cell was inserted into the designed phantom to acquire the force reading. The readings acquired by the load cell go through the instrumentation amplifier to amplify the small readings. The amplification is helpful during feature extraction in MATLAB as the waveform characteristics of the lower-force layers are more prominent. The amplified signal is then sent to MATLAB for signal processing and classification using the Classification Learner app that is built in MATLAB. As for the display screen, it is used to display the classifier results when testing the phantom.

III. RESULTS AND DISCUSSION

First, the calibration curve was plotted in Excel to observe the linearity of the system as shown in Fig. 3. This calibration was used to examine the pressure values of different layers on the needle tip. Hence, the average pressure value obtained from each layer is plotted in Fig. 8, where the best trendline was obtained with Polynomial option with an order of 5. The error bar of each layer force is illustrated as well, where the variation of the readings is examined.

The load cell calibration was done to ensure accurate results. Fortunately, the calibration curve showed a linear relationship between the applied force and the output voltage.

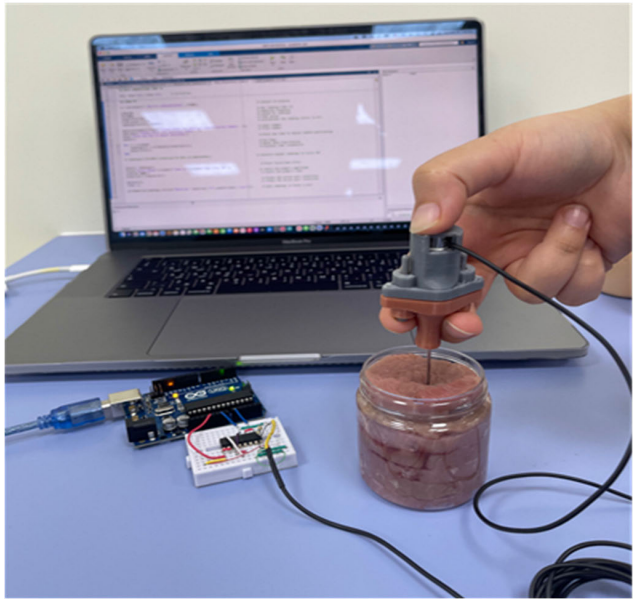

FIGURE 7. Experimental setup.

Hence, the linearity of a sensor helps minimize the uncertainty of its output scale, which was guaranteed in this procedure. After that, the average results of forces that were taken from each layer were recorded using load cell and MATLAB software. The outcome of the study in [25] was used to analyze the obtained results.

From Fig. 8, it was proven that the LF phantom was always exerting the highest force on the needle tip, whereas the ES is the lowest. It is important to note that the researchers in [3] and [26] observed that the exerted force drops as the needle is being inserted to the ES layer. ES is mainly composed of loose adipose connective tissue that is filled with blood vessels; hence, this type of tissue does not resist the injection of fluid.

The pressure of spinal cord layers was estimated in MATLAB first over 20 trials of each layer. Then, the results of these trials were grouped based on their features to plot the forces of each layer and its amplitudes respectively. Hence, these features were varied according to the recorded layer. For instance, the pressure of the skin layer on the needle tip was recorded 20 times and then the result's features were extracted. Similarly, this procedure was done to the remaining

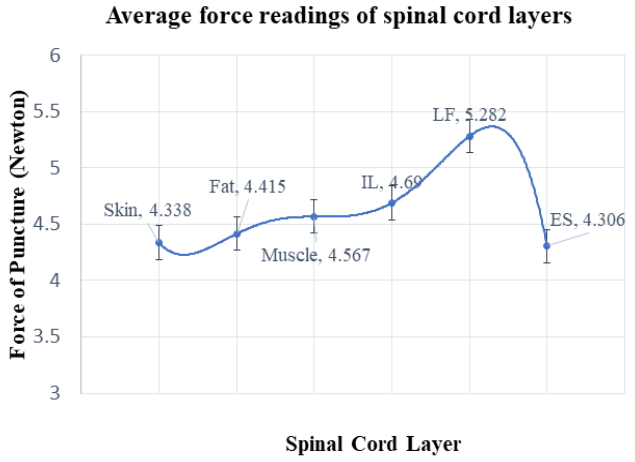

FIGURE 8. Average pressure value obtained from each layer.

layers. Then, a table of features was created to start the classification based on it, as shown in Table 2. Knowing that new columns representing the class number were added next to each layer feature.

SPSS Statistics Software was used to test the accuracy of the classification. SPSS software is produced by IBM® that offers a comprehensive range of features, including advanced statistical analysis, a diverse collection of machine learning algorithms, text analysis, open-source tools, integration with big data systems, and effortless deployment into various applications. Therefore, the accuracy of the features using Linear Distribution Classifier was observed and studied accordingly. Multiple classification trials were done to improve accuracy. One way to improve accuracy is by increasing the number of trials so that the classifier can understand the behavior of the readings and determine their distribution. Another way is by increasing the number of features, as more features will give the classifier more data to read and examine. As a result, 50 trials were taken, and 20 features were extracted. The overall accuracy validation increased to 77.1%. Knowing that 88% of skin readings are classified as skin, and 95.9% of ES readings are classified correctly. Although other layers are still not high enough compared to the accurate classification, they are still classified correctly when the materials are tested in the lab. Nevertheless, other classification applications were used to improve the overall accuracy such as the Bilayered Neural Network in MATLAB. Thus, the Bilayered Neural Network classifier was used in MATLAB using Classification Learner where the accuracy testing result was 86.7%, as shown in Fig. 9.

To ensure that the obtained accuracy test percentage is almost repeatable, the feature table was inputted to the Classification Learner many times where the percentage of the Bilayered Neural Network classifier remained fixed. Other classifiers were considered as well, as seen in Table 3. It is clear that the percentage of accuracy was above 80% in all trials with different classifiers.

TABLE 2. Table of classification features.

Feature Number	Classification Feature
1	Mean Value
2	Standard Deviation
3	Root Mean Square
4	Variance
5	Skewness
6	Kurtosis
7	Maximum Value
8	Minimum Value
9	Range of Readings
10	Peak-to-peak Value
11	Crest Value
12	Clearance Factor
13	Impulse Factor
14	Shape Factor
15	Margin Factor
16	Zero Crossing Rate
17	Length of Waveform
18	Mean of Absolute Deviation
19	Mean of Absolute Value
20	Mean of Absolute Deviation

TABLE 3. Classification results of different classifiers.

Classifier	Accuracy Test
Linear Discriminant Analysis	80.0 %
Ensemble	80.0 %
SVM	83.0 %
Kernel	83.0 %
Bilayered Neural Network	86.7 %

After that, the Bilayered Neural Network classifier output was exported to MATLAB workspace to start testing the layers as explained in the previous section. To ensure that our results are satisfied, and the classification of each layer was done correctly, a data comparison was done. As stated in section 3.2, previous research outcomes were compared and analyzed thoroughly. The relation of forces of the spinal cord were observed and taken into consideration when validating the results. Where it was guaranteed that the obtained results were within the expected range since it satisfied the force-layer relation. Knowing that the phantom was designed based on the general characteristics of each layer, the exerted force on the needle tip was expected to be at its lowest value when testing the ES phantom, given the previously explained reasons. Fortunately, this is what was obtained from multiple trials of the designed classification system. Hence, the design system can successfully evaluate the force of puncture and can easily detect the drop-in forces to state the ES layer.

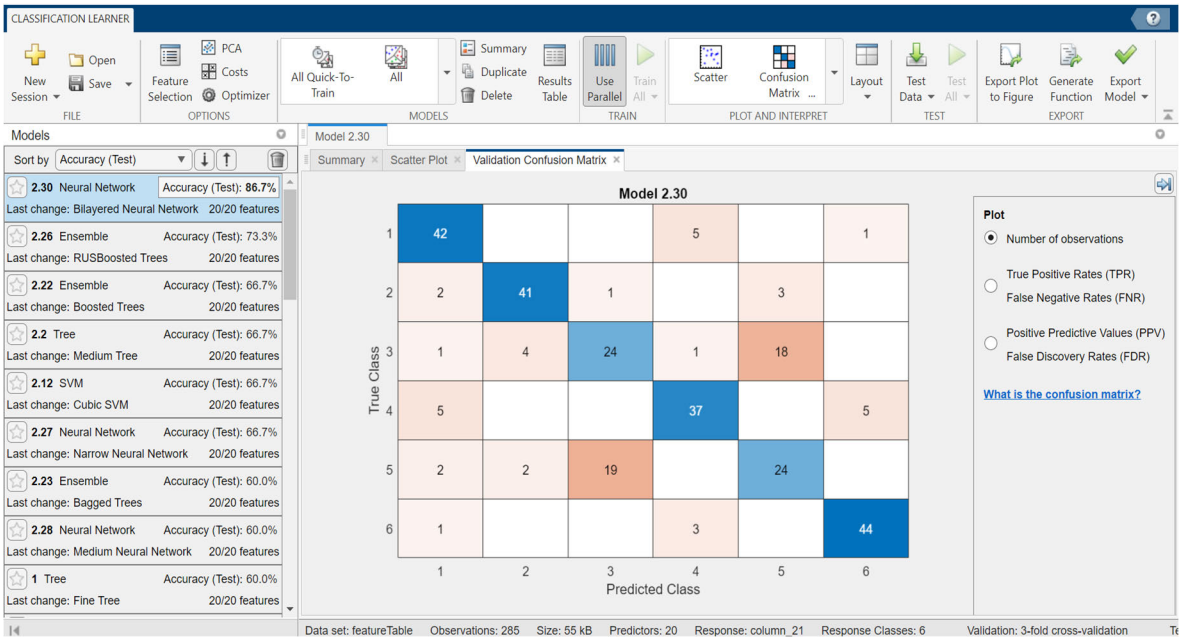

FIGURE 9. Classification learner output comparing classification accuracy of different classifiers.

IV. CONCLUSION

In conclusion, this paper aimed to design a high-accuracy, relatively low-cost epidural needle with force puncture guidance. The goal was to improve the success rate of LPs at the first try. Thus, reducing the risks and side effects of repeating the procedure, as well as decreasing the procedure's failure rate. The identification system was built using a button load cell that was mounted above the spinal needle and secured using a needle casing. Due to the limitations, the tests were carried out on a phantom that mimics the force properties of the different spinal tissue layers. The phantom was used to collect a database of a couple of hundred readings that were used to build the classifier after the sought-after features were extracted. The classifier was built using the recorded database and provided our system with 86.7% accuracy. The accuracy is acceptable given that it is above 80% and that can be further improved by taking more readings for the database. After the classifier was built and exported, new readings were taken and classified into one of the six spinal layers. Although the design was successful at performing its required objectives, there is still plenty of room for improvement. First, the classification accuracy can be enhanced further by taking more readings to build the database. A more accurate phantom may also be tested to provide more repeatable readings with less variability, as the phantoms used in this devices testing may have had slight differences, especially in the meat layers, as a new phantom was needed to be made every week. The device's accuracy may also be improved by selecting a more sensitive, and possibly more expensive load cell.

APPENDIX A
DATA ACQUISITION CODE

```
%% DATA ACQUISITION CODE %%
clc; clear all; close all; % Initialize
%% Code %%
s=serialport('COM3;, 57600); % Connect to Arduino
time=10; % Set reading
time (s)
Fs=1000; % Sampling
frequency
Length=Fs*time; % Length of
readings
t=(0:Length-1)/Fs; % Time vector
readings=zeros(1,Length); % Initializes the
reading vector to 0's
material=num2str(input('Please enter the material
classification number: ')); % Layer number
num=input('Please enter the recording number: '); %
Trial number
disp('Press any key to begin recording');
pause(); % Gives you time
to adjust needle positioning
for i = 1:Length % For-loop
readings(i) = str2double(readline(s)); % Reads data
from Arduino
disp((i/Fs)); % Displays time (stopwatch)
end
plot(t, readings); % Plots forcetime curve
title('Force Signal');xlabel('Time
(s)');ylabel('Amplitude');
ylim([-20 1000]); % Limits the graph's amplitude
xlim([-0.3 (time+0.3)]); % Limits the graph's time
delete(s); % Closes the serial port connection
clear s; % Closes the serial port connection
writematrix(readings,(strcat("Material
",material,"/T",num2str(num),".csv"))); % Save
readings in excel (.csv)
```

APPENDIX B
MODULE TRAINING CODE

```
%% TRAINING SYSTEM %%
clc; clear all; close all; %Initialize
%% Code %%
X = []; %Initialize the feature matrix
Y = []; %Initialize the label vector
folder = ''; %Define the folder containing the data
classNames = {'Material 1', 'Material 2', 'Material
3'}; %Define the names of the three layers
% Define the names of the 20 text files
fileNames = {'T1.csv', 'T2.csv', 'T3.csv', 'T4.csv',
'T5.csv', ...
'T6.csv', 'T7.csv', 'T8.csv', 'T9.csv',
'T10.csv','T11.csv', 'T12.csv', 'T13.csv', 'T14.csv',
'T15.csv', ...
'T16.csv', 'T17.csv', 'T18.csv', 'T19.csv',
'T20.csv'};
for class = 1:length(classNames) % Loop the classes
for file = 1:length(fileNames) % Loop each file in
selected class
data = readtable(fullfile(folder, classNames{class},
fileNames{file})); % Load the data from file
readings = table2array( data ) ;
% Create filter
window_size = 20; % Select size of window/mask
window = ones(1, window_size)/window_size; % Set
filter coefficients=1
readings = filter(window, 1, readings); % Run the
filter
% Feature Extraction
mean_value = mean(readings); % Find mean
std_value = std(readings); % Find standard deviation
rms_value = rms(readings); % Find rms
var_value = var(readings); % Find variance
skewness_value = skewness(readings); % Find skewness
kurtosis_value = kurtosis(readings); % Find kurtosis
max_value = max(readings); % Find maximum value
min_value = min(readings); % Find minimum value
range_value = range(readings); % Find the range of the
readings
peak2peak_value = peak2peak(readings); % Find peak to
peak
crest_factor = max(readings)/rms(readings); % Find
crest value
clearance_factor = rms(readings)/mean(abs(readings));
% Set clearance
impulse_factor = max(abs(readings))/rms(readings); %
Set impulse factor
shape_factor = rms(readings)/abs(mean(readings)); %
Set shape factor
margin_factor =
max(abs(readings))/mean(abs(readings));% Set margin
factor
zc_rate =
sum(abs(diff(sign(readings))))/(2*numel(readings)); %
Find zero crossing rate
wave_length = sum(abs(diff(readings))); % Find length
of waveform
mean_ad = mad(readings); %Find mean of absolute
deviation
mean_av = mean(abs(readings)); % Find mean of absolute
value
median_ad = median(abs(readings - median(readings)));
% Find median of absolute deviation
% Create a row vector of features
row = [mean_value std_value rms_value var_value
skewness_value kurtosis_value max_value
min_value range_value peak2peak_value crest_factor
clearance_factor impulse_factor shape_factor
margin_factor zc_rate wave_length mean_ad mean_av
median_ad];
X = [X; row]; %Set the row vector to the feature
matrix
Y = [Y; class]; %Create labels for the current class
end
end
featureTable = [X, Y]; %Combine the feature matrix and
label vector into a single table
```

APPENDIX C
SOFTWARE CLASSIFICATION CODE

```
%% AI CLASSIFICATION SYSTEM %%
clear;clc;
load("C:\Users\najwa\OneDrive\سطح
المكتب\classifiers\Bilayered_NN_867_PERC_3_5.mat");
  %%
s = serialport('COM5', 57600);
time = 10;
% Set reading time (s)
Fs = 1000;
% Sampling frequency
Length = Fs*time;
% Length of readings
t = (0:Length-1)/Fs;
% Time vector
readings = zeros(1, Length);
% Initializes the reading vector to 0's
% Gives you time to adjust needle positioning
for i = 1:Length
% For-loop
    readings(i) = str2double(readline(s));
% Reads data from Arduino
    disp((i/Fs));
% Displays time (stopwatch)
end
delete(s);                                          %
Closes the serial port connection
clear s;                                            %
Closes the serial port connection

% Create filter
window_size = 20;                                   %
Select size of window/mask
window = ones(1, window_size)/window_size;          %
Set filter coefficients=1
readings = filter(window, 1, readings);             %
Run the filter
% Extracting features
mean_value = mean(readings);
% Find mean
std_value = std(readings);
% Find standard deviation
rms_value = rms(readings);
% Find rms
var_value = var(readings);
% Find variance
skewness_value = skewness(readings);
% Find skewness
kurtosis_value = kurtosis(readings);
% Find kurtosis
max_value = max(readings);
% Find maximum value
min_value = min(readings);
% Find minimum value
range_value = range(readings);
% Find the range of the readings
peak2peak_value = peak2peak(readings);
% Find peak to peak
crest_factor = max(readings)/rms(readings);
% Find crest value
clearance_factor = rms(readings)/mean(abs(readings));
% Set clearance
impulse_factor = max(abs(readings))/rms(readings);
% Set impulse factor
shape_factor = rms(readings)/abs(mean(readings));
% Set shape factor
margin_factor =
max(abs(readings))/mean(abs(readings)); % Set margin
```

```
factor
zc_rate =
sum(abs(diff(sign(readings))))/(2*numel(readings)); %
Find zero crossing rate
wave_length = sum(abs(diff(readings)));
% Find length of waveform
mean_ad = mad(readings);                                %
Find mean of absolute deviation
mean_av = mean(abs(readings));                          %
Find mean of absolute value
median_ad = median(abs(readings - median(readings)));
% Find median of absolute deviation
iq_range = iqr(readings);                               %
Find interquartile range
ma_signal = sum(abs(readings));                         %
Find magnitude area of signal
% Create a row vector of features
Features = [mean_value std_value rms_value var_value
skewness_value kurtosis_value max_value min_value
range_value peak2peak_value crest_factor
clearance_factor impulse_factor shape_factor
margin_factor zc_rate wave_length mean_ad mean_av
median_ad];

% Load the neural network classification file
yfit = (trainedModel.predictFcn(Features));
s1 = serialport('COM3',9600);
 % Apply classification
fopen(s1);

j=1;
while (j~=0)
    if yfit==1
        Prediction = "Material 1";
        value='1';

    elseif yfit==2
        Prediction = "Material 2";
        value='2';

    elseif yfit==3

        Prediction = "Material 3";
        value='3';

    elseif yfit==4
        Prediction = "Material 4";
        value='4';

    elseif yfit==5
        Prediction = "Material 5";
    value='5';

    elseif yfit==6
        Prediction = "Material 6";
        value='6';
    end
    fwrite(s1, value);
    pause(1);
    fwrite(s1, value);
    j=0;
end
pause(2);
fclose(s1);
delete(s1);
%Closes the serial port connection
```

REFERENCES

[1] H. Elsharkawy, A. Sonny, and K. Chin, "Localization of epidural space: A review of available technologies," *J. Anaesthesiol. Clin. Pharmacol.*, vol. 33, no. 1, p. 16, 2017, doi: 10.4103/0970-9185.202184.

[2] A. Khlebtovsky, S. Weitzen, I. Steiner, A. Kuritzky, R. Djaldetti, and S. Yust-Katz, "Risk factors for post lumbar puncture headache," *Clin. Neurol. Neurosurg.*, vol. 131, pp. 78–81, Apr. 2015, doi: 10.1016/j.clineuro.2015.01.028.

[3] A. M. Dogliotti, "Research and clinical observations on spinal anesthesia: With special reference to the peridural technique," *Anesthesia Analgesia*, vol. 12, no. 1, pp. 59–65, Jan. 1933.

[4] S. Ambastha, S. Umesh, S. Dabir, and S. Asokan, "Spinal needle force monitoring during lumbar puncture using fiber Bragg grating force device," *J. Biomed. Opt.*, vol. 21, no. 11, Nov. 2016, Art. no. 117002, doi: 10.1117/1.jbo.21.11.117002.

[5] C. Wang, P. Calle, J. C. Reynolds, S. Ton, F. Yan, A. M. Donaldson, A. D. Ladymon, P. R. Roberts, A. J. de Armendi, K.-M. Fung, S. S. Shettar, C. Pan, and Q. Tang, "Epidural anesthesia needle guidance by forward-view endoscopic optical coherence tomography and deep learning," *Sci. Rep.*, vol. 12, no. 1, May 2022, Art. no. 9057, doi: 10.1038/s41598-022-12950-7.

[6] S. Y. Kang, O. N. Kashlan, R. Singh, R. Rane, N. M. Adsul, S. C. Jung, J. Yi, H. S. Cho, H. S. Kim, I.-T. Jang, and S.-H. Oh, "Advantages of the combination of conscious sedation epidural anesthesia under fluoroscopy guidance in lumbar spine surgery," *J. Pain Res.*, vol. 13, pp. 211–219, Jan. 2020, doi: 10.2147/jpr.s227212.

[7] T. Grau, R. W. Leipold, S. Fatehi, E. Martin, and J. Motsch, "Real-time ultrasonic observation of combined spinal–epidural anaesthesia," *Eur. J. Anaesthesiol.*, vol. 21, no. 1, pp. 25–31, Jan. 2004, doi: 10.1017/s026502150400105x.

[8] B. Carotenuto, A. Ricciardi, A. Micco, E. Amorizzo, M. Mercieri, A. Cutolo, and A. Cusano, "Smart optical catheters for epidurals," *Sensors*, vol. 18, no. 7, p. 2101, Jun. 2018, doi: 10.3390/s18072101.

[9] M. Althobaiti, S. Ali, N. G. Hariri, K. Hameed, Y. Alagl, N. Alzahrani, S. Alzahrani, and I. Al-Naib, "Recent advances in smart epidural spinal needles," *Sensors*, vol. 23, no. 13, p. 6065, Jun. 2023, doi: 10.3390/s23136065.

[10] T. Moore, "A survey of the mechanical characteristics of skin and tissue in response to vibratory stimulation," *IEEE Trans. Man Mach. Syst.*, vol. MMS-11, no. 1, pp. 79–84, Mar. 1970, doi: 10.1109/tmms.1970.299966.

[11] B. S. Simpson, M. Burns, R. P. Dick, and L. Saager, "Epidural needle guidance using viscoelastic tissue response," *IEEE J. Transl. Eng. Health Med.*, vol. 10, pp. 1–11, 2022, doi: 10.1109/JTEHM.2022.3152391.

[12] C. Arzola, S. Davies, A. Rofaeel, and J. C. A. Carvalho, "Ultrasound using the transverse approach to the lumbar spine provides reliable landmarks for labor epidurals," *Anesthesia Analgesia*, vol. 104, no. 5, pp. 1188–1192, 2007, doi: 10.1213/01.ane.0000250912.66057.41.

[13] T. Grau, R. W. Leipold, R. Conradi, and E. Martin, "Ultrasound control for presumed difficult epidural puncture," *Acta Anaesthesiologica Scandinavica*, vol. 45, no. 6, pp. 766–771, Jul. 2001, doi: 10.1034/j.1399-6576.2001.045006766.x.

[14] Q. Tang, C.-P. Liang, K. Wu, A. Sandler, and Y. Chen, "Real-time epidural anesthesia guidance using optical coherence tomography needle probe," *Quantum Imag. Med. Surg.*, vol. 5, no. 1, pp. 118–124, Feb. 2015, doi: 10.3978/j.issn.2223-4292.2014.11.28.

[15] S. P. Lin, M. S. Mandell, Y. Chang, P. T. Chen, M. Y. Tsou, K. H. Chan, and C. K. Ting, "Discriminant analysis for anaesthetic decision-making: An intelligent recognition system for epidural needle insertion," *Brit. J. Anaesthesia*, vol. 108, no. 2, pp. 302–307, Feb. 2012, doi: 10.1093/bja/aer369.

[16] F. H. Halvorsen, O. J. Elle, and E. Fosse, "Simulators in surgery," *Minimally Invasive Therapy Allied Technol.*, vol. 14, nos. 4–5, pp. 214–223, Jan. 2005, doi: 10.1080/13645700500243869.

[17] T. R. Coles, D. Meglan, and N. W. John, "The role of haptics in medical training simulators: A survey of the state of the art," *IEEE Trans. Haptics*, vol. 4, no. 1, pp. 51–66, Jan. 2011, doi: 10.1109/TOH.2010.19.

[18] R. A. Lee, T. C. R. V. van Zundert, J. J. M. van Koesveld, A. A. J. van Zundert, R.-J. Stolker, P. A. Wieringa, and S. P. Gatt, "Evaluation of the Mediseus epidural simulator," *Anaesthesia Intensive Care*, vol. 40, no. 2, pp. 311–318, Mar. 2012, doi: 10.1177/0310057x1204000215.

[19] J. Kallewaard, J. Paz-Solis, P. De Negri, M. Canós-Verdecho, H. Belaid, S. Thomson, D. Abejón, J. Vesper, V. Mehta, P. Rigoard, P. Maino, S. Love-Jones, I. Peña, S. Bayerl, C. Perruchoud, R. Bougeard, C. Mertz, Y. Pei, and R. Jain, "Real-world outcomes using a spinal cord stimulation device capable of combination therapy for chronic pain: A European, multicenter experience," *J. Clin. Med.*, vol. 10, no. 18, p. 4085, Sep. 2021, doi: 10.3390/jcm10184085.

[20] ATO.com. *Subminiature Load Cell, Button Type, 3kg/5kg/10kg/20kg/50kg/100kg*. Accessed: Jul. 22, 2023. [Online]. Available: https://www.ato.com/subminiature-load-cell-3kg-to-100kg
[21] *Working With a Load Cell and an Arduino*. Accessed: Jul. 22, 2023. [Online]. Available: https://edg.uchicago.edu/tutorials/load_cell/
[22] A. Beisenova, A. Issatayeva, C. Molardi, and D. Tosi, "Fiber Bragg grating sensor-based optical guidance system for epidural catheter," in *Proc. IEEE SENSORS*, Oct. 2018, pp. 1–4, doi: 10.1109/ICSENS.2018.8630284.
[23] The Arduino Team, Arduino Documentation. *State Change Detection (Edge Detection) for Pushbuttons*. Accessed: May 22, 2023. [Online]. Available: https://docs.arduino.cc/built-in-examples/digital/StateChangeDetection
[24] N. Agnihotri, "How to use ILI9486 driver 3.5 TFT LCD touch screen with Arduino," Engineers Garage, Tech. Rep., Accessed: May 22, 2023. [Online]. Available: https://www.engineersgarage.com/arduino-ili9486-driver-3-5-inch-tft-lcd-touch-screen/
[25] H. Li, Y. Wang, Y. Li, and J. Zhang, "A novel manipulator with needle insertion forces feedback for robot-assisted lumbar puncture," *Int. J. Med. Robot. Comput. Assist. Surg.*, vol. 17, no. 2, p. e2226, Apr. 2021, doi: 10.1002/rcs.2226.
[26] G. Capogna, *Epidural Technique In Obstetric Anesthesia*, 2020.

MURAD ALTHOBAITI received the B.Sc. and M.Sc. degrees in biomedical engineering from Wright State University, Dayton, OH, USA, in 2011 and 2013, respectively, and the Ph.D. degree in biomedical engineering from the University of Connecticut, USA. Currently, he is an Associate Professor with the Biomedical Engineering Department, Imam Abdulrahman Bin Faisal University, Saudi Arabia. His research interests include optical imaging, NIR spectroscopy, biomedical instrumentation, and cancer detection.

YARA ALAGL received the B.Sc. degree in biomedical engineering from Imam Abdulrahman Bin Faisal University, Dammam, Saudi Arabia, in 2023. Her research interests include biomedical instrumentation and biomaterials.

NAJWA ALZAHRANI received the Graduate degree from Imam Abdulrahman Bin Faisal University (IAU), in 2023. She is a passionate individual with a keen interest in the field of biomedical engineering. She excelled in her coursework and aspires to make a positive impact on healthcare technology.

SARA ALZAHRANI received the bachelor's degree in biomedical engineering from Imam Abdulrahman Bin Faisal University, Dammam, Saudi Arabia, in June 2023.

SAJID ALI received the Ph.D. degree in mechanical engineering from the King Fahd University of Petroleum and Minerals, Dhahran, Saudi Arabia, in 2018. He is currently an Assistant Professor with the Mechanical and Energy Engineering Department, Imam Abdulrahman Bin Faisal University, Dammam, Saudi Arabia. He has published more than 30 peer reviewed journals and conference publications. His research interests include renewable energy, structural dynamics, vibration, finite element modeling, and roll-to-roll manufacturing.

NASIR G. HARIRI received the B.S. degree from the Mechanical and Production Engineering Department, King Abdulaziz University, Jeddah, Saudi Arabia, the M.S. degree in mechanical engineering with mechatronics concentration from Western New England University, Massachusetts, USA, in 2015, and the Ph.D. degree from the Mechanical Engineering Department, Florida Institute of Technology (FIT), Melbourne, USA, in 2018. He is currently an Associate Professor with the Mechanical and Energy Engineering Department, Imam Abdulrahman Bin Faisal University (IAU). His work is directly involved and specialized in the design and implementation of various control and mechatronics systems in the mechanical and renewable energy fields.

KAMRAN HAMEED received the B.S. degree (Hons.) in biomedical engineering from the Sir Syed University of Engineering and Technology, Karachi, Pakistan, in 2006, and the M.E. degree in electronics engineering (micro system design) from the NED University of Engineering and Technology, Karachi, Pakistan, in 2009. He was associated with several teaching positions at emerging university, from 2006 to 2013, Pakistan. Since July 2013, he has been a Lecturer with Imam Abdulrahman Bin Faisal University. His research interests include embedded system design, electronic design automation, control system design, bioinstrumentation, and medical image processing.

IBRAHEEM AL-NAIB (Senior Member, IEEE) was born in Mosul, Iraq. He received the B.Sc. and M.Sc. degrees in electronics and communication from Mosul University, Mosul, in 1993 and 1996, respectively, and the Dr.-Ing. (Ph.D.) degree in electrical engineering, information technology, and physics from Technische Universität Braunschweig, Braunschweig, Germany, in 2009.

He has held teaching university appointments with Ajman and Sharjah Universities, United Arab Emirates, between 2002 and 2005. From 2010 to 2013, he was a Postdoctoral Research Fellow with the Centre Énergie Matériaux Télécommunications, Institut National de la Recherche Scientifique, Varennes, Québec, Canada, and from 2013 to 2015, he was a Postdoctoral Fellow with Queen's University, Kingston, ON, Canada. From 2015 to 2019, he was an Assistant Professor with Imam Abdulrahman Bin Faisal University, Dammam, Saudi Arabia, where he became as an Associate Professor, in April 2019. He is currently a Full Professor with the King Fahd University of Petroleum & Minerals, Dhahran, Saudi Arabia. He has authored and coauthored 76 journal articles, 85 conference papers, and two book chapters. His research interests include biosensing, terahertz spectroscopy for biomedical applications, and high-quality factor planar metamaterials.